http://dx.doi.org/10.5935/0103-5053.20130042

J. Braz. Chem. Soc., Vol. 24, No. 2, 327-335, 2013.
Printed in Brazil - ©2013 Sociedade Brasileira de Química
0103 - 5053 $6.00+0.00

Article

Coprecipitation of Safrole Oxide with Poly(3-hydroxybutyrate-*co*-3-hydroxyvalerate) in Supercritical Carbon Dioxide

Ernandes T. Tenório-Neto,[a] Expedito L. Silva,[a] Thelma S. Pacheco Cellet,[a] Elisangela P. Silva,[a] Elton Franceschi,[b] Lúcio C. Filho,[c] Adley F. Rubira[a] and Marcos H. Kunita*[,a]

[a]Departamento de Química, Universidade Estadual de Maringá, Av. Colombo, 5790, 87020-900 Maringá-PR, Brazil

[b]Instituto de Tecnologia e Pesquisa (ITP), Universidade Tiradentes, Campus Farolândia, Av. Murilo Dantas, 300, 49032-490 Aracaju-SE, Brazil

[c]Departamento de Engenharia Química, Universidade Estadual de Maringá, Av. Colombo, 5790, 87020-900 Maringá-PR, Brazil

5-(Oxiran-2-ilmetil)-1,3-benzodioxol ou epóxi-safrol (SO) vem sendo estudado ao longo dos anos devido a suas propriedades dependentes da concentração, como indução à apoptose e transdiferenciação celular. A coprecipitação do SO com um polímero biodegradável e biocompatível, poli(3-hidroxibutirato-*co*-3-hidroxivalerato) (PHBV), foi realizada utilizando a técnica de dispersão de solução aumentada por fluídos supercríticos (SEDS). Um planejamento fatorial 2^{4-1} foi realizado para investigar os efeitos das condições experimentais (pressão, vazão de solução e de antissolvente e concentrações de PHBV e SO) na eficiência do processo e na morfologia dos coprecipitados. Para o material obtido SO/PHBV, foram observadas formas esféricas e fibrosas, sendo as morfologias dependentes das condições experimentais. Os mecanismos de liberação controlada de epóxi-safrol para os materiais esféricos foram diferentes dos materiais fibrosos. Análise térmica mostrou uma diminuição na temperatura de máxima velocidade de degradação (T_{max}) em relação ao PHBV, atribuída à presença de SO e à morfologia da amostra.

In recent years, 5-(oxiran-2-ylmethyl)-1,3-benzodioxole or safrole oxide (SO) has been widely studied due to its concentration dependent properties, such as cellular apoptosis inducing activity and cell transdifferentiation. Coprecipitation of SO with a biodegradable and biocompatible polymer, poly(3-hydroxybutyrate-*co*-3-hydroxyvalerate) (PHBV), were performed using solution enhanced dispersion by supercritical fluids technique (SEDS). A 2^{4-1} factorial design was carried out to investigate the effect of processing parameters (pressure, solution flow, anti-solvent flow and concentrations of PHBV and SO) on the process efficiency and microparticle morphology. Both fibrous and spherical shapes were observed for coprecipitated SO/PHBV, which were dependent on the experimental-processing conditions. Controlled release mechanisms of SO to spherical materials were different from fibrous materials. Thermal analysis showed a decrease in the temperature of maximum weight loss rate (T_{max}) of PHBV, attributed to the presence of SO and sample morphology.

Keywords: SEDS, coprecipitation, safrole oxide, PHBV, factorial design

Introduction

Apoptosis (programmed cell death) has been characterized as fundamental cellular activity to maintain the physiological balance of the organism by eliminating unwanted cells. Activation of apoptotic pathways by chemotherapeutic agents has been one of the treatments for cancer therapy.[1] Safrole oxide (SO) has been studied in recent years due to its anti-angiogenesis and apoptosis-inducing activity in the *in vitro* cancer therapy.[2-5] In those studies, it has been reported that concentrations of safrole oxide below 10 μg mL^{-1} induce human umbilical vein endothelial cell transdifferentiation to 5-hydroxytryptaminergic neuron-like cells,[6] and that concentrations of approximately 20 μg mL^{-1} induce apoptosis in the human oral cancer HSC3.[7,8] However, in concentrations of SO higher than 20 μg mL^{-1}, it plays a

*e-mail: mkunita@gmail.com

role as a genotoxic agent.[9] Therefore, controlled amounts of safrole oxide released in a given system by a biodegradable polymer, for example, can improve its therapeutic action and thus increasing its potential.

Poly(hydroxyalkanoates) (PHAs), which are synthesized by microorganisms under unbalanced growth conditions, are generally biodegradable, with good biocompatibility, being technologically attractive for use as an encapsulating agent.[10,11] Poly(3-hydroxybutyrate) (PHB) and poly(3-hydroxybutyrate-*co*-3-hydroxyvalerate) (PHBV) are the most extensively known PHAs. However, PHB is very brittle which restricts its application.[12] In the biomedical field, PHBV has been used to develop various bio-implant products in both the tissue engineering and the encapsulation protection of controlled delivery of drugs.[13-16]

The conventional techniques of coprecipitation and encapsulation such as spray-drying, freeze-drying and interfacial polymerization can often result in product damage, degradation of thermo-sensitive compound and contamination with the solvent. In this sense, several techniques based on supercritical technology, employing mainly carbon dioxide as either solvent or anti-solvent, have been developed to overcome the drawbacks of the traditional methods and to meet the current demands of pharmaceutical sector in view of growing interest in producing more sophisticated release systems.[17-20]

Solution enhanced dispersion by supercritical fluid (SEDS) technology has been used to produce fine particles.[21] SEDS has been also used to micronize diverse materials, such as lactose, β-carotene, polymers, pharmaceuticals and composites.[22,23]

The main focus of this work is on developing microparticles based on SO and PHBV with different shapes, using a factorial design 2^{4-1}, and on investigating the effect of its morphology on both the thermal behavior and the drug release profile.

Experimental

Reagents

Safrole oxide (SO) was synthesized by reaction of safrole with *m*-chloroperoxybenzoic acid in dichloromethane (DCM) and subsequently purified by silica gel column chromatography (400-200 Mesh).[7] Carbon dioxide (99.9% in liquid phase) was purchased by White Martins (Maringá, Brazil). Poly(3-hydroxybutirate-*co*-3-hydroxyvalerate) (PHBV) with 8% HV and M_n = 218.9 kg mol^{-1}, M_w/M_n = 1.156 was supplied by PHB Industrial S.A. (São Paulo, Brazil). All materials used were prepared without further purification.

Factorial design

A 2^{4-1} fractional factorial with a central point, which is represented by the superior (+1) and inferior (−1) levels and central point (0), was built to investigate the influence of independents variables on the coprecipitation of safrole oxide with PHBV in dichloromethane by SEDS technology.

The independent variables that could affect on the synthesis of SO/PHBV microparticles, under supercritical conditions, such as pressure (P), supercritical carbon dioxide ($scCO_2$) flow rate (Q_{CO2}), liquid solution flow rate (Q_S) and initial concentration of the solution (I_C), were the factors selected to build the factorial design. The I_C factor was defined by the following expression:

$$I_C = \frac{\text{Concentration of HBV}}{\text{Concentration of safrole oxide}} \quad (1)$$

where higher values of I_C indicate higher PHBV concentrations than SO, while low I_C values indicate lower PHBV concentrations in relation to safrole oxide.

Other experimental parameters were used as follows: temperature (40 °C), washing time (2 h, Q_{CO2} 40 g min^{-1}) and nozzle diameter (184 μm). The ranges of the factors (for which the values of the variables were selected) were chosen on the basis of preliminary precipitation tests. These experiments were carried out using the static synthetic method in a high-pressure variable-volume view cell.

Table 1 shows the range chosen for each factor. The concentration ranges of PHBV and safrole oxide in DCM were 30-40 and 4.0-5.0 mg mL^{-1} at room temperature, respectively.

Table 1. Factors and levels selected to build the 2^{4-1} factorial design with a central point

Independent variable	Factor	Level		
		(–1)	(0)	(+1)
Pressure / MPa	(A)	8.0	12.0	16.0
Ic	(B)	6	8	10
Q_{CO2} / (g min^{-1})	(C)	30	35	40
Q_S / (g min^{-1})	(D)	5	10	15

The 2^{4-1} factorial design allowed the evaluation of the process efficiency (PE). It also allowed the observation of the influence of the precipitation conditions on both the morphology and the particle size, which are the most important solid-state properties defined by crystallization process.[23,24]

Validation of the statistical model

To validate the statistical model, a random experiment named run 12 was carried out using the following experimental conditions: P = 8.0 MPa (–1), Ic = 10 (+1), Q_{CO2} = 40 g min^{-1} (+1) and Q_S = 15 g min^{-1} (+1).

Precipitation procedure and apparatus

A scheme of the apparatus (Thar Technology, model SAS 200) used for coprecipitation of SO and PHBV is shown in Figure 1. It consists of two high pressure pumps (THAR P-350 and THAR P-50 for injections of $scCO_2$ and solution, respectively), a precipitating chamber of 316 stainless steel with an internal volume of 2000 mL (vessel 1) involved by a thermal jacket, a separating chamber of 316 stainless steel with an internal volume of 500 mL (vessel 2) to separate the carbon dioxide from residual solution, and an automatic back pressure regulator (ABPR) to control the output flow, maintaining the pressure constant. All the factors that have any influence on the process, such as pressure (P), temperature (T) and flow (Q), are controlled by software (Process Suite).

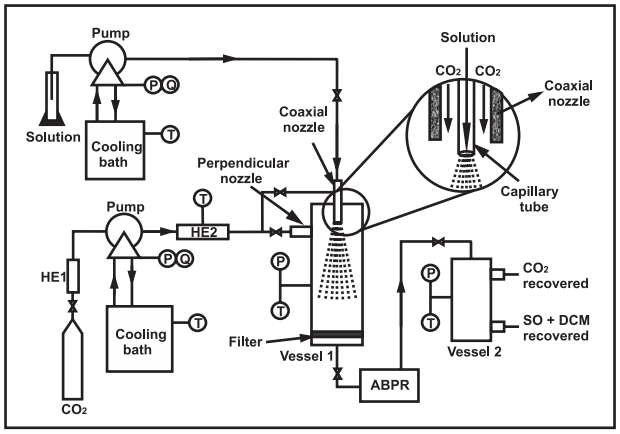

Figure 1. Scheme illustrating the apparatus used in the precipitations of SO and PHBV: pressure (P), temperature (T), flow (Q), heat exchanger (HE) and automatic back pressure regulator (ABPR).

The carbon dioxide was injected into the vessel 1 up to the desired pressure. After the pressure and temperature were adjusted, the liquid solution (DCM + SO + PHBV) was pumped to the vessel 1 through the coaxial nozzle. This solution was pumped inside a fused silica capillary tube with an internal diameter of 184 μm, whereas $scCO_2$ was pumped by two ways: (*i*) through outside capillary tube, dispersing the solution (coaxial nozzle), and (*ii*) by a perpendicular nozzle with the aim of increasing the turbulence inside the vessel 1, and to promote a more intense mixing between the solution and anti-solvent.

The experiment was ended when the solution was completely pumped, after that, the carbon dioxide was continuously injected into the vessel 1 with a stream of 40 g min^{-1} (washing time) for 2 h. The precipitating chamber was slowly depressurized until reaching the ambient pressure. Then, the obtained particles were collected by a paper filter that was placed on a sintered metal filter.

Analysis and characterization

The precipitated particles were analyzed by a scanning electron microscope (SEM, Shimadzu, model SS 550 Superscan). SEM images were made by applying an accelerating voltage of 10 kV and current of 30 mA. The samples were sputter-coated with a thin layer of gold on their surface before SEM visualization. Particle sizes were measured by Image-Pro Plus software. Particle size distribution curves were elaborated by measuring particle size for 400 particles using Statistica® 8.0 software. The responses for factorial design and drug release tests were verified by an UV-Vis spectrophotometer (Varian, Cary 50 Conc.). Two calibration curves were elaborated using UV-Vis spectroscopy for SO in different solvents: (*i*) in dichloromethane for responses of factorial design, and (*ii*) in hydroalcoholic solution containing 62.5% ethanol and 37.5% water for drug release tests, according to guidelines for drug dissolution and drug release found in the 23rd United States Pharmacopeia Convention. The absorbance was measured at 287 nm ($n \rightarrow \pi^*$ aromatic ring transitions of safrole oxide).[4]

PE was the response chosen to elaborate factorial design. A sample of coprecipitated SO/PHBV was weighed in an analytical balance with precision 0.00001 g (Denver Instruments, model AA-200DS). The powder was dissolved in DCM and the absorbance was measured at 287 nm. The amount of safrole oxide in the sample was calculated by comparing the results with the calibration curve (absorbance × concentration). PE was estimated according to the following equation:

$$\text{Process efficiency (PE)} = \frac{\text{Percentage of safrole oxide in the sample}}{\text{Theoretical percentage of safroleoxide}} 100 \qquad (2)$$

Differential scanning calorimetry (DSC) experiments were performed using a DSC Q-20, TA Instruments. Dry nitrogen was employed to purge the DSC cell with a stream of 50 mL min^{-1}. Samples of approximately 6 mg were weighed and sealed in the DSC pans of aluminum and placed into the DSC cell. They were heated from room temperature up to 200 °C at a heating rate of 10 °C min^{-1}.

The samples were kept at 200 °C for 5 min to remove the thermal history. Subsequently, the samples were cooled to –10 °C at a cooling rate of 10 °C min^{-1}. Then, the samples were again heated to 200 °C at a heating rate of 10 °C min^{-1}. The thermal parameters were obtained from the second heating scan. The degree of crystallinity of both PHBV and PHBV/SO (X_C in %) were estimated according to equation 3:

$$X_C = \frac{\Delta H_{fus}}{\Delta H^0_{fus}\, W_{PHB}} 100\% \quad (3)$$

where ΔH_{fus} is the fusion enthalpy of the sample, W_{PHB} is the weight fraction of PHB in the sample, and ΔH^0_{fus} is the fusion enthalpy for 100% crystallized PHB, that is 146 J g^{-1}.[25]

Samples of approximately 6 mg were weighed in open platinum pans for TG measurements using a Shimadzu TGA-50 Thermogravimetric Analyzer. The nitrogen stream was 20 mL min^{-1} at heating rate of 10 °C min^{-1}, starting from room temperature up to 600 °C.

In vitro release study

The release profiles of SO were determined by means of fractional release (C_t/C_∞) as a function of time. Value of release exponent (n) was determined through equation 4 (Peppa's mathematical model), where k is a constant incorporating structural and geometric characteristics of the sample.[26-28]

$$\frac{C_t}{C_\infty} = k\, t^n \quad (4)$$

Equation 4 was used to characterize the first 60% of the release behavior. It is important to report that n is a parameter depending on the geometrical shape of the polymer matrix.[27] The conceptual meanings of n for the different geometrical shapes of polymer matrix such as cylinder, thin film and sphere are summarized in Table 2. In this study, run 1 and run 12 were regarded as cylindrical and spherical shapes, respectively.

Table 2. Values of diffusional exponent (n) for the polymer matrix with different geometrical shapes[27]

Diffusional exponent (n)			Transport mechanism
Thin film	Cylinder	Sphere	
0.50	0.45	0.43	Fickian diffusion
$0.50 < n < 1.00$	$0.45 < n < 0.89$	$0.43 < n < 0.85$	anomalous transport
1.00	0.89	0.85	macromolecular relaxation

Release tests were performed using 100 mg of SO/PHBV microparticles dispersed in 30 mL of hydroalcoholic solution with 62.5% ethanol (v/v) (23rd USP Convention). Then, the mixture was introduced into a dialysis tube. After being carefully closed, suspension-filled dialysis tube was fixed at the bottom of a glass reactor containing 220 mL hydroalcoholic solution at 37 °C. The external solution was stirred at 50 rpm using a paddle stirrer. Aliquots of 3 mL were collected from the external solution at specified periods, and then adsorption readings were made at 287 nm. Afterwards, the aliquots were brought back into the reactor.

Results and Discussion

High-pressure variable view cell

Figure 2a shows a ternary system under pressure of 8.0 MPa at 40 °C with 0.75 mass fraction of CO_2 (wCO_2). Ternary system consists of a solid phase with PHBV core, a viscous and dense liquid phase, possibly rich in DCM + SO, and a fluid phase, possibly rich in $scCO_2$. There was no change in the number of components on the ternary system when the pressure was increased to 16.0 MPa (Figure 2b).

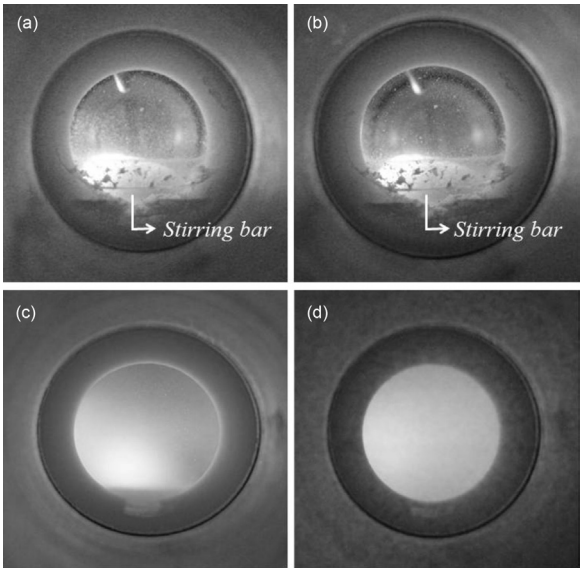

Figure 2. Experimental phase equilibrium using high-pressure variable-volume view cell for the solution with 40 mg mL^{-1} of PHBV, and 4 mg mL^{-1} of SO in DCM at 40 °C. Conditions: (a) P = 8.0 MPa, wCO_2 = 0.75; (b) P = 16.0 MPa, wCO_2 = 0.75; (c) P = 8.0 MPa, wCO_2 = 0.50 and (d) P = 16.0 MPa, wCO_2 = 0.50.

In order to investigate the influence of the amount of anti-solvent on the system, the mass fraction of CO_2 was decreased to 0.50 (Figure 2c). In such conditions, there was no precipitation of PHBV, even with an increase of pressure to 16.0 MPa, shown in Figure 2d. The experimental

conditions for coprecipitation of SO/PHBV described in Figures 2a and 2b were chosen to avoid loss of safrole oxide in $scCO_2$, because SO is liquid at room temperature.

Statistical treatment

Table 3 shows the experiments (runs) elaborated for design matrix. Factorial design with a central point was used to estimate the experimental error.

Table 3. Process efficiency (PE) (responses) for 2^{4-1} factorial design

Run	Coded factor				Experimental PE / %	Predicted PE / %
	(A)	(B)	(C)	(D)		
01	(–1)	(+1)	(+1)	(–1)	3.30	3.27 ± 0.09
02	(+1)	(+1)	(–1)	(–1)	1.81	1.84 ± 0.09
03	(+1)	(+1)	(+1)	(+1)	1.92	1.95 ± 0.09
04	(–1)	(+1)	(–1)	(+1)	1.11	1.08 ± 0.09
05	(0)	(0)	(0)	(0)	1.21	1.73 ± 0.03
06	(–1)	(–1)	(–1)	(–1)	1.99	2.02 ± 0.09
07	(0)	(0)	(0)	(0)	1.34	1.73 ± 0.03
08	(–1)	(–1)	(+1)	(+1)	1.07	1.10 ± 0.09
09	(+1)	(–1)	(–1)	(+1)	1.22	1.19 ± 0.09
10	(0)	(0)	(0)	(0)	1.41	1.73 ± 0.03
11	(+1)	(–1)	(+1)	(–1)	1.42	1.39 ± 0.09

An empirical model was built by regression of experimental data with the use of software Design Expert 7.0®. With the empirical model, it was possible to determine the predicted PE. The general expression from empirical fitted model is described as follows:

$$PE_{predicted}\ (\%) = +1.73 - 0.14A + 0.30B + 0.20C - 0.40D - 0.12AC + 0.38AD \quad (5)$$

The values of predicted PE are near to those of experimental PE, which is an indicative of a good fitting. The best results for PE were obtained at pressure of 8.0 MPa.

The analysis of variance (ANOVA), obtained from the fit of PE, is shown in Table 4. The *p*-value was used to judge the significance level for each term. It is insignificant when its *p*-value is larger than 0.05 (for a confidence level of 95%).[29] It is important to report that the lack-of-fit was not statistically significant.

Table 4. Analysis of variance[a] data for 2^{4-1} factorial design

Source	Sum of squares	df	Mean square	*p*-Value
Model	3.74	6	0.62	0.0029
Residual	0.029	3	9.542×10^{-3}	
Lack-of-fit	8.065×10^{-3}	1	8.065×10^{-3}	0.4692
Pure error	0.021	2	0.010	
Total	4.13	10		
$R^2 = 0.992$				

[a]Confidence level 95% ($p < 0.05$), df = degree of freedom.

This statistical model explains 99% of the total variability. It was validated using a random experiment (run 12). Where, the PE experimental and predicted values by the statistical model were 1.87 ± 0.02% and 1.71 ± 0.09%, respectively.

Figure 3 shows the three-dimensional graphs of the combined effect of pressure and Q_{CO2} in higher I_C values. Better results for PE are obtained in lower pressures, shown in Figure 3a. This can be explained in terms of solubility. The solubility of safrole oxide in the system increases as pressure increases. There is then a decrease in PE due to the mass loss of SO in the mixture flow.[12,30]

In the experimental conditions under which Q_S is increased, the interaction between pressure and Q_{CO2} showed a different effect (Figure 3b). An increase in the pressure results in a better PE. This is attributed to the

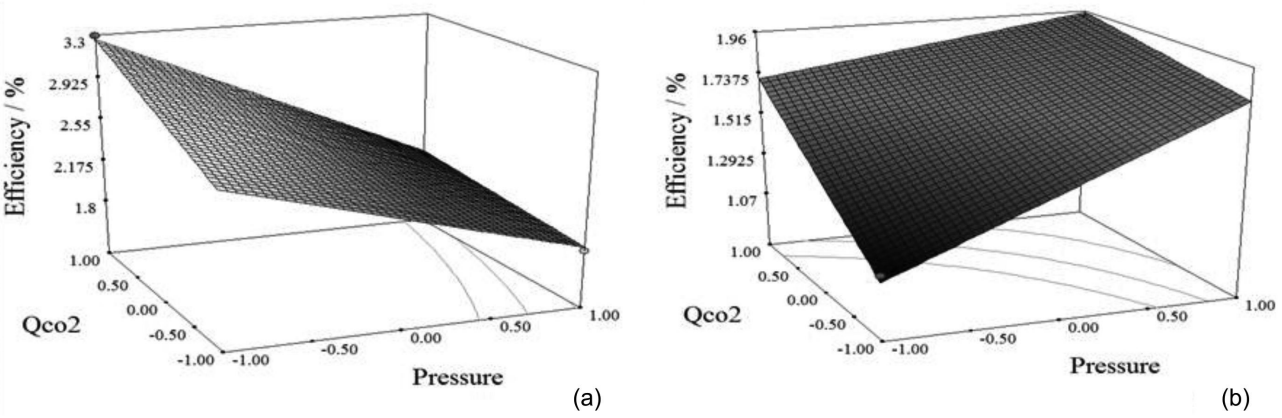

Figure 3. The combined effect of pressure and Q_{CO2} in I_C (+) on PE: (a) Q_S = 5 g min^{-1} and (b) Q_S = 15 g min^{-1}.

increased amount of anti-solvent inside the precipitating chamber, which may be a determinant factor in the coprecipitation of the SO/PHBV particles.

The influence of the amount of anti-solvent on the system can be better understood by phase equilibrium, shown in Figure 2. The concept used here is analogous to the procedures for solubilization and precipitation of polymers.[31] Higher amount of anti-solvent in the system decreases the polymer-solvent interaction, favoring the polymer-polymer interactions. Figure 2a shows the three phases at equilibrium: solid PHBV core, liquid viscous and dense and fluid. On the other hand, when the amount of solvent was increased, the PHBV core was solubilized (Figure 2c). There is then reduction of nucleation and thereby decreasing coprecipitation. Finally, the higher value of I_C (which indicates high PHBV concentration) favored coprecipitation due to the increased nucleation points inside the chamber.[32]

Morphology and size distribution

The effect of some conditions on the particle diameter and morphology was investigated. Figure 4 shows the SEM images of safrole oxide and PHBV microparticles precipitated by SEDS. The samples showed different particle morphologies, attributed to different experimental conditions used in SEDS. The unprocessed polymer (Figure 4a) has irregular particles with different diameters, ranging from 30 to 340 μm. Figure 4b shows the SEM images of polymer precipitated by SEDS without safrole oxide (*p*-PHBV). The precipitation conditions were adjusted as follows: (*i*) 8.0 MPa, (*ii*) Q_{CO2} 40 g min^{-1} and (*iii*) Q_S 15g min^{-1}. *p*-PHBV showed uniform distribution of particle diameter, comparatively to commercial sample. SEM images of Figures 4b, 4c, 4e and 4f show that the particles are smaller than the unprocessed polymer, showing a mean diameter lower than 5 μm. Also, it is observed agglomerated particles with relatively spherical forms and fibers.

The formation of fibers is characteristic of concentrated solutions, which is due to two main factors: (*i*) high viscosity in the droplet and (*ii*) insufficient solubility of the liquid solvent in the supercritical anti-solvent during the washing process. The first factor hinders the diffusion of $scCO_2$ into to the droplets affecting the evaporation of organic solvent and the second factor contributes to a coalescence mechanism.[12,30,33]

Changes on the experimental conditions induce changes on the particle morphology. For instance, in the experimental conditions under which Q_S is reduced, the spherical morphology of the sample (Figure 4c) changed to fibrous morphology (Figure 4f). In the experimental condition which is represented in Figure 2a, there is a solid-liquid-fluid equilibrium, thereby the presence of liquid (probably rich in DCM) would have influenced on the coalescence of particles.

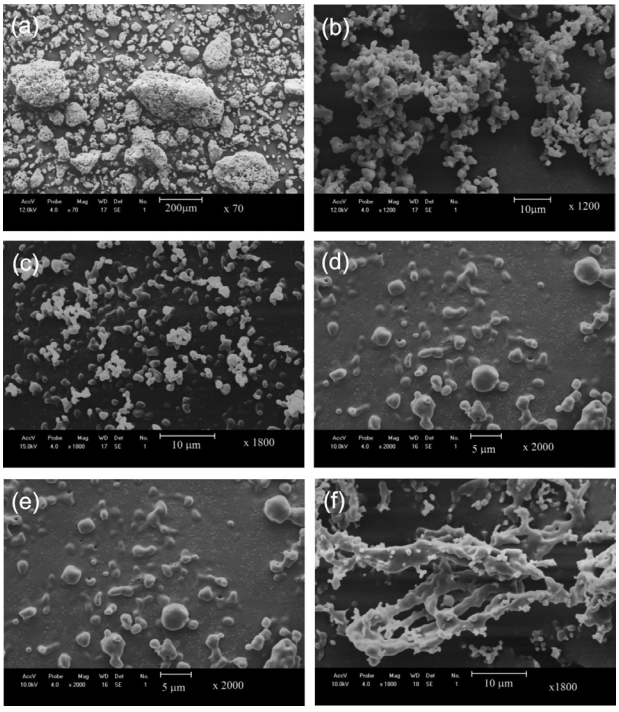

Figure 4. SEM micrographs of safrole oxide and PHBV microparticles precipitated in SEDS: (a) commercial PHBV, (b) PHBV precipitated by SEDS (*p*-PHBV), (c) run 12, (d) run 08, (e) run 03 and (f) run 01.

The effect of the I_C value was evaluated. Comparing run 12 with run 3, no significant change was observed on morphology. However, the pressure effect was observed when run 12 (Figure 4c) is compared with run 3 (Figure 4e). When the pressure was changed from 8.0 to 16.0 MPa, it was observed that the spherical morphology (run 12) changed to a blend of fibers and spheres (run 3). In this case, an increase in the pressure leads an increase in the viscosity in the system. As a result, formation of fiber was favored. Anyway, the description of a ternary diagram, especially when polymers are involved, is an important approach to better understand such behavior.

The particle diameter (PD) of precipitated material ranged from 0.79 to 2.36 μm and the variation coefficient (VC) ranged from 0.305 to 0.467% (Table 5). The fibers were produced in runs 1, 2 and 9. In all other experiments, interconnected particles with relatively spherical forms were obtained, which are polymer structures different from the unprocessed PHBV.

Thermal characterization

Figure 5 shows the DSC curves of the second heating scan for PHBV and PHBV/SO microparticles. It has been

Table 5. Experimental results of mean particle diameter (PD) and variation coefficient (VC)[a]

Run	PD / μm	VC[a] / %
Unprocessed PHBV	94.43	46.8
p-PHBV[c]	2.36	30.5
01[d]	–	–
02[b]	–	–
03[d]	–	–
04[c]	1.21	38.8
05[b,e]	1.19	36.1
06[b]	1.20	46.7
07[b,e]	0.97	37.1
08[c]	1.83	43.7
09[d]	–	–
10[b,e]	1.00	36.0
11[c]	0.79	29.1
12[c]	1.24	31.5

[a]VC is defined as the ratio between the standard deviation and the mean particle size; [b]blend of fibers and spheres; [c]spheres; [d]fibers; [e]central points.

Table 6. Thermal properties obtained from DSC and TGA curves for pure PHBV and coprecipitated PHBV/SO

Run	SO[b] / %	T_{max} / °C	T_{onset} / °C	X_C / %
p-PHBV	–	282.7	252.7	24.9
01	0.30	276.8	245.3	22.3
02	0.16	274.8	243.0	24.4
03	0.18	272.3	238.4	23.9
04	0.10	272.9	242.2	24.5
05[a]	0.14	275.5	244.7	23.7
06	0.28	276.0	244.6	23.6
07[a]	0.16	274.7	244.4	25.7
08	0.16	271.7	241.0	23.8
09	0.17	273.6	241.0	23.3
10[a]	0.16	278.5	247.7	24.1
11	0.20	276.2	242.2	23.7
12	0.17	259.2	229.1	23.6

[a]Center points; [b]percentage of safrole oxide in the sample (w SO/w sample).

reported that the double melting peaks in PHBV can be linked to the formation of two crystalline phases with different sizes, thickness and/or structural ordering that can be formed through a melting, recrystallization and remelting process.[25,34,35]

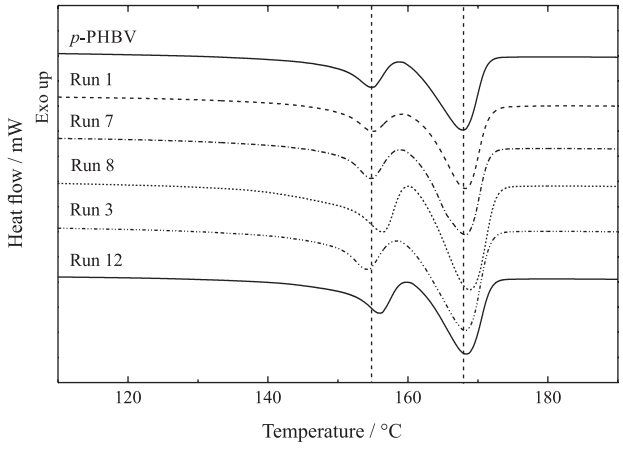

Figure 5. DSC curves of PHBV + SO precipitated in different conditions by SEDS process.

As described in Table 6, the presence of safrole oxide did not affect the melting point and crystallization process of PHBV significantly.

The first peak (Figure 5) corresponds to imperfect crystals. In the runs 8 and 12, there was only a small shift. The changes on the melting temperatures were related to changes in the lamellar thickness of the crystal and its distribution inside the sample.[10,36]

The influence of safrole oxide in the PHBV/SO particles was investigated by TGA analysis (Figure 6). All samples showed only a weight loss step between 210-300 °C and no char residue was detected. This finding is in accordance with the random chain scission reaction.[37,38]

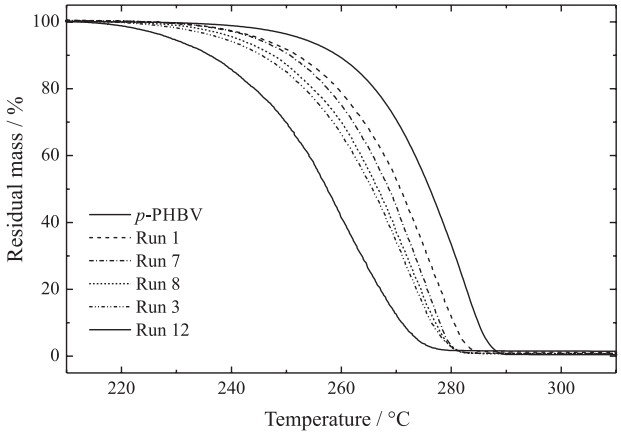

Figure 6. Thermogravimetric curves of PHBV + SO precipitated in different conditions by SEDS process.

As a general trend, in the presence of safrole oxide, the curves are shifted to lower temperatures, indicating a decrease in the thermal stability of microparticles compared to that of pure PHBV. The maximum temperature of weight-loss rate (T_{max}) was obtained from first derivative curve. The data were listed in Table 6.

The initial temperature of decomposition (T_{onset}) corresponded to the temperature in which the polymer has 5% of degradation. This effect was less prominent with the

introduction of safrole oxide (shifts of ca. 10 °C). However, in the run 12 (Table 6), there were significant changes on both T_{onset} and T_{max} values. Comparing these results (run 12) with run 1 and run 6, it is observed that the percent amount of safrole oxide in the run 12 is two times lower than that in the run 1 and run 6. However, run 12 showed both T_{onset} and T_{max} values lower than other samples.

Degradation curves, shown in Figure 6, also can be related to morphology. For example, fibrous samples have smaller shifts on T_{max} than spherical samples, while blends of fibers and spheres showed intermediate values on T_{max}. This suggests that the morphology possesses a greater influence on the degradation temperature than the amount of safrole oxide.

In vitro release of safrole oxide

Safrole oxide release from SO/PHBV microparticles was investigated. It was chosen samples from run 1 (Figure 7a) and run 12 (Figure 7b), which showed fibrous and spherical morphologies, respectively.

The value of *n* was estimated from linear slope of the logarithmical curve of C_t/C_∞ plotted against t. The *n* values were 0.4363 and 0.8102 for run 12 (sphere) and run 1 (fiber), respectively. These results indicate that the transport mechanism for SO/PHBV microparticles were anomalous. However, fibrous matrix trends to macromolecular relaxation, while spherical matrix trends to Fickian diffusion.

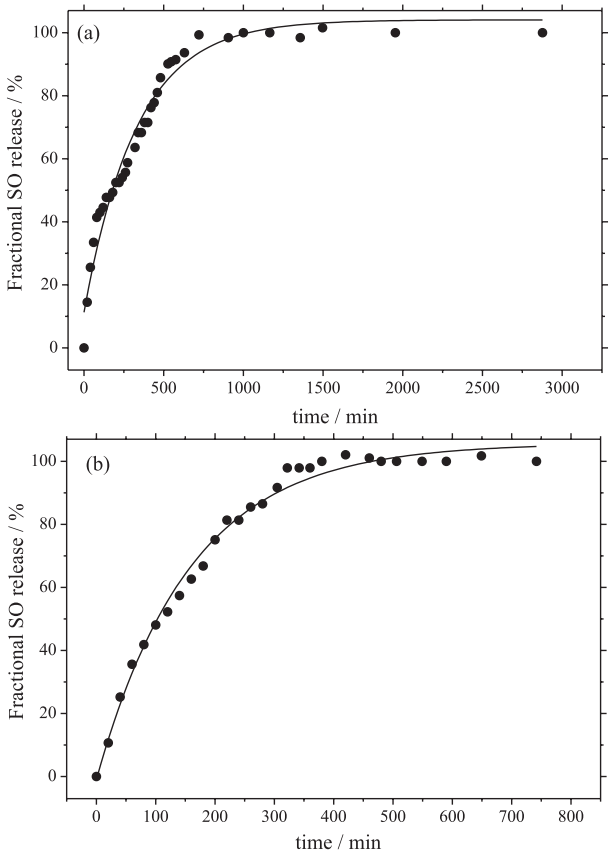

Figure 7. Time dependent fractional release curve of safrole oxide from PHBV/SO microparticles in hydroalcoholic solution at 37 °C: (a) spherical matrix (run 12) and (b) fibrous matrix (run 1).

The release time of SO from spherical matrix (Figure 7) was lower than fibrous matrix. About 90% of SO on run 1 was released in the first 500 min. On the other hand, the release time for the same amount of SO (run 12) was three times higher.

In order to investigate if the difference on safrole oxide release was associated with encapsulation percentage, the samples of coprecipitated SO/PHBV (runs 1 and 12) were suspended in ethanol and maintained under sonication for 2 min to extract unencapsulated SO. Then, the resultant suspension was filtered and dried under room temperature for 42 h. Afterwards, the dried samples were weighed and dissolved in dichloromethane and the absorbance was measured. Each experiment was carried out in triplicate. SO was not detected in fibrous matrix (run 1) and approximately 93% of safrole oxide was detected in spherical matrix (run 12). These results are in accordance to type of both mechanism and release time of safrole oxide.

Conclusions

In this work, it was investigated the coprecipitation of safrole oxide on PHBV from dichloromethane solutions by SEDS using supercritical carbon dioxide as anti-solvent. Supercritical fluid coprecipitation technology is a useful method for the preparation of pharmaceutical forms. Fractional factorial design showed that the best pressure condition for PE was 8.0 MPa. PE ranged from 1.10-3.30%, and despite low percentages, the amount of SO found in the polymeric matrix was more than enough for use in controlled release systems, and for transdifferentiation experiments or tests of apoptosis in epithelial cells.

The microparticle morphology was dependent on supercritical conditions. Spherical particles were obtained using P = 8.0 MPa, Q_{CO2} = 40 g min^{-1} and Q_S = 15 g min^{-1}. Fibrous particles were produced changing Q_S to 5 g min^{-1}. The spherical particles became fibers by coalescence. Fibers showed the best results in PE owing to longer contact time with SO during its coalescence. In such a case, ternary diagram description, especially when polymers are involved, is an important approach to better understand this type of behavior. The melting temperature and crystallization degree were not affected by the presence of safrole oxide, which can indicate only the formation of a physical mixture between SO and PHBV. The amount

of SO and the morphology of the sample influenced the thermal degradation of PHBV. However, the effect of morphology was the most prominent.

It was observed that fibrous matrix was three times faster than spherical matrix on release of SO. This difference on release is due to the amount of encapsulated SO.

Supplementary Information

Supplementary data about characterization of safrole oxide and calibration curve are available free of charge at http://jbcs.sbq.org.br as a PDF file.

Acknowledgment

The authors thank Coordenação de Aperfeiçoamento de Pessoal de Nível Superior (CAPES) for the financial support and master degree fellowship.

References

1. Zhao, Y. F.; Kong, Q. Z.; *Chem.-Biol. Interact.* **2008**, *174*, 19.
2. Zhao, J.; Miao, J. Y.; Zhao, B.; Zhang, S.; Yin, D.; *Vasc. Pharmacol.* **2005**, *43*, 69.
3. Du, A. Y.; Zhao, B. X.; Miao, J. Y.; Yinc, D. L.; Zhang, S. L.; *Bioorg. Med. Chem.* **2006**, *14*, 2438.
4. Su, L.; Zhao, B. X.; Lv, X.; Wang, N.; Zhao, J.; Zhang, S.; Miao, J. Y.; *Life Sci*. **2007**, *80*, 999.
5. Du, A.; Zhao, B. X.; Yin, D.; Zhang, S.; Miao, J. Y.; *Bioorg. Med. Chem. Lett*. **2006**, *16*, 81.
6. Su, L.; Zhao B. X.; Lv. X.; Zhao, J.; *Bioorg. Med. Chem. Lett*. **2007**, *17*, 3167.
7. Su, L.; Zhao, J.; Zhao, B. X.; Zhang, S. L.; Miao, J. Y.; *Int. J. Biochem. Cell Biol*. **2011**, *43*, 1512.
8. Yu, F. S.; Yang, J. S.; Yu, C. S.; Lu, C. C.; Chiang, J. H.; Lin, C. W.; Chung, J. G.; *J. Dent. Res.* **2011**, *90*, 168.
9. Chiang, S. Y.; Lee, P. Y.; Lai, M. T.; Shen, L. C.; Chung, W. S.; Huang, H. F.; Wu, K. Y.; Wu, H. C.; *Mutat. Res., Genet. Toxicol. Environ. Mutagen.* **2011**, *726*, 234.
10. Yang, F.; Qiu, Z.; *Ind. Eng. Chem. Res.* **2011**, *50*, 11970.
11. Bazzo, G. C.; Lemos-Senna, E.; Gonçalves, M. C.; Pires, A. T. N.; *J. Braz. Chem. Soc.* **2008**, *19*, 914.
12. Franceschi, E.; Cesaro, A. M.; Feiten M.; Ferreira, S. R. S.; Dariva, C.; Kunita, M. H.; Rubira, A. F.; Muniz, E. C.; Corazza, M. L.; Oliveira, J. V.; *J. Supercrit. Fluids* **2008**, *47*, 259.
13. Farago, P. V.; Raffin, R. P.; Pohlmann, A. R.; Guterres, S. S.; Zawadzki, S. F.; *J. Braz. Chem. Soc.* **2008**, *19*, 1298.
14. Wang, W.; Cao, J.; Lan, P.; Wu, W.; *J. Appl. Polym. Sci.* **2012**, *124*, 1919.
15. Priamo, W. L.; Cezaro, A. M.; Bentti, S. C.; Oliveira, J. V. J.; Ferreira, S. R. S.; *J. Supercrit. Fluids* **2011**, *56*, 137.
16. Chen, W.; Tong, Y. W.; *Acta Biomater.* **2012**, *8*, 540.
17. Celiktas, O. Y.; Senyay, D.; *Ind. Eng. Chem. Res*. **2010**, *49*, 7017.
18. Lang, Z. M.; Hong, H. L.; Han, L. M.; Zhu, N.; Suo, Q. L.; *Chem. Eng. Technol.* **2012**, *35*, 362.
19. Mauricio, M. R.; Manso, F. C. G.; Kunita, M. H.; Velasco, D. S.; Bento, A. C.; Muniz, E. C.; Carvalho, G. M.; Rubira, A. F.; *Compos. Part A-Appl. S.* **2011**, *42*, 757.
20. Mauricio, M. R.; Silva, T. S.; Kunita, M. H.; Muniz, E. C.; Carvalho, G. M.; Rubira, A. F.; *J. Mater. Sci.* **2012**, *47*, 4965.
21. Mezzomo, N.; Paz, E.; Maraschin, M.; Martin, A.; Cocero, M. J.; Ferreira, S. R. S.; *J. Supercrit. Fluids* **2012**, *66*, 342.
22. Zhang, Y. Z.; Liao, X. M.; Yin, G. F.; Yuan, P.; Huang, Z. B.; Gu, J. W.; Yao, Y. D.; Chen, X. C.; *Powder Technol*. **2012**, *221*, 343.
23. Franceschi, E.; Cezaro, A.; Ferreira, S. R. S.; Kunita, M. H.; Muniz, E. C.; Rubira, A. F.; Oliveira, J. V.; *Open Chem. Eng. J*. **2010**, *4*, 11.
24. Montes, A.; Tenorio, A.; Gordillo, M. D.; Pereyra, C. M.; Ossa, E. J. M.; *Ind. Eng. Chem. Res*. **2011**, *50*, 2343.
25. Yu, H. Y.; Qin, Z. Y.; Wang, L. F.; Zhou, Z.; *Carbohydr. Polym*. **2012**, *87*, 2447.
26. Siepmann, J.; Peppas, N. A.; *Adv. Drug Delivery Rev.* **2001**, *48*, 139.
27. Guilherme, M. R.; Fajardo, A.; Moia, T. A.; Kunita, M. H.; Gonçalves, M. C.; Rubira, A. F.; Tambourgi, E. B.; *Eur. Polym. J.* **2010**, *46*, 1465.
28. Silva, A. R.; Zaniquelli, M. E. D.; Baratti, M. O.; Jorge, R. A.; *J. Braz. Chem. Soc.* **2010**, *21*, 214.
29. Zhao, H.; Tonkyn, R. G., Barlow, S. E.; Peden, C. H.; Koel, B. E.; *Ind. Eng. Chem. Res*. **2006**, *45*, 934.
30. Subra, P.; Jestin, P.; *Ind. Eng. Chem. Res.* **2000**, *39*, 4178.
31. Yu, Z. Q.; Chow, P. S.; Tan, R. B. H.; *Ind. Eng. Chem. Res.* **2006**, *45*, 438.
32. Wagner, P. E.; Strey, R.; *J. Phys. Chem.* **2001**, *105*, 11656.
33. Reverchon, E.; *J. Supercrit. Fluids* **1999**, *15*, 1.
34. Duan, B.; Wang, M.; Zhou, W-Y.; Cheung, W.-L.; *Polym. Eng. Sci.* **2011**, *51*, 1580.
35. Ye, H. M.; Wang, Z.; Wang, H. H.; Chen, G. Q.; Xu, J.; *Polymer* **2010**, *51*, 6037.
36. Chang, L.; Chou, Y. H.; Woo, E. M.; *Colloid Polym. Sci.* **2011**, *289*, 199.
37. Carli, L. N.; Crespo, J. S.; Mauler, R. S.; *Compos. Part A-Appl. S.* **2011**, *42*, 1601.
38. Thiré, R. M. S. M.; Arruda, L. C.; Barreto, L. S.; *Mat. Res*. **2011**, *14*, 340.

Submitted: October 15, 2012
Published online: February 27, 2013